JOURNAL AFRICAIN DES SCIENCES
VOL. 3, **11** (2026) 34-52

https://jafrisci.org

ISSN (online) : 3107-0949 ; ISSN (print) : 3107-0930

OPEN ACCESS

RESEARCH ARTICLE

Article Info.:
Received : 12th August 2026
Accepted : 23rd September 2026
Published : 26th September 2026

PETROGRAPHIC CHARACTERIZATION AND U-Pb DATING OF THE LAMPA METARHYOLITES FROM THE TSHELA AREA (Kongo Central Province, Democratic Republic of the Congo)

Trésor Kawaya Hubert [1,2,*], Yann Waku Mpaka [1], Luc Tack [2], Marc Poujol3, Mathias Potvin [2], Augustin Dekoninck [4,5], Albert Tienge Ongendangenda [1], Ridi Diakondua [1], Nicole Kitambala [6], Camille François [2]

https://doi.org/10.70237/jafrisci.2026.v3.i11.04

Résumé

Les métarhyolites de Lampa, affleurant dans la région de Tshela et rattachées à la Formation d'Inga (Groupe de Seke-Banza, Supergroupe de l'Ouest-Congo, République Démocratique du Congo), s'inscrivent dans une succession volcanique felsique vraisemblablement d'âge tonien développée le long de la marge occidentale du Craton du Congo. Bien que cette succession soit reconnue à l'échelle régionale, sa variabilité pétrographique interne et son évolution tectono-métamorphique postérieure restent peu contraintes. Cette étude combine les observations de terrain, la pétrologie et la géochronologie in situ U-Pb sur titanite par LA-ICP-MS afin de réévaluer la nature et l'évolution de ces roches volcaniques felsiques. Trois faciès volcaniques reliques sont observés : des métarhyolites à matrice abondante, des métarhyolites riches en (phéno)cristaux et un faciès pyroclastique distinct, reconnu ici pour la première fois. Ces faciès conservent des caractères volcaniques primaires malgré des degrés variables de séricitisation, chloritisation, recristallisation, et déformation liée au remaniement panafricain lors de la formation de la chaîne Ouest-Congolienne. Les titanites de deux de nos échantillons définissent un âge U-Pb combiné de 559 ± 15 Ma, interprété comme l'âge de cristallisation des titanites au cours de cet événement orogénique. Ces résultats apportent de nouvelles contraintes pétrographiques et géochronologiques sur l'évolution des roches issues du magmatisme felsique dans la région de Tshela.

Mots-clés: Métarhyolites de Lampa ; géochronologie U-Pb sur titanite ; magmatisme felsique tonien ; Chaîne Ouest-Congolienne

Abstract

The Lampa metarhyolites, exposed in the Tshela region and assigned to the Inga Formation (Seke-Banza Group, West Congo Supergroup, Democratic Republic of the Congo), form part of a probably Tonian felsic volcanic succession developed along the western margin of the Congo Craton. Although this succession is recognized at the regional scale, its internal petrographic variability and subsequent tectono-metamorphic evolution remain poorly constrained. This study integrates field observations, petrography, and in situ LA-ICP-MS U-Pb titanite geochronology to reassess the nature and evolution of these felsic volcanic rocks. Three relict volcanic facies are identified: matrix-rich metarhyolites, (pheno)crystal-rich metarhyolites, and distinct pyroclastic facies recognized here for the first time. These facies preserve primary volcanic characteristics despite variable degrees of sericitization, chloritization, recrystallization, and deformation associated with Pan-African reworking during the development of the West Congo Belt. Titanite grains from two of our samples yield a combined U-Pb age of 559 ± 15 Ma, interpreted as the timing of titanite crystallization during this orogenic event. These results provide new petrographic and geochronological constraints on the evolution of rocks derived from felsic magmatism in the Tshela region.

Keywords: Lampa metarhyolites; titanite U-Pb geochronology; Tonian felsic magmatism; West Congo Belt.

1. Introduction

Felsic volcanic rocks in ancient volcano-sedimentary successions are important markers of extensional basin development, crustal magmatism, and stratigraphic correlation. Their primary architecture may include coherent lava domains, crystal-rich facies, volcaniclastic components, flow-related textures, and devitrified matrices, which are commonly used to reconstruct volcanic processes

Corresponding Author: *hubert.kawaya@unikin.ac.cd* ***(T. K. Hubert)***

Copyright : © The Author(s) Published under a Creative Commons Attribution 4.0 International Licence (CC BY 4.0)

[1] *Department of Geosciences, University of Kinshasa, Kinshasa, Democratic Republic of the Congo*
[2] *Royal Museum for Central Africa, Tervuren, Earth Sciences Department, GeoRes4Dev project, Belgium*
[3] *CNRS, Géosciences Rennes, UMR 6118, Université de Rennes, Rennes, France*
[4] *Service de Génie Minier, Département Mines-Géologie, Faculté Polytechnique de Mons (FPMs), Université de Mons, Rue du Joncquois 53, Mons, 7000, Belgium.*
[5] *G-Time Laboratory, Department of Geosciences, Environment and Society, Université libre de Bruxelles (ULB), Av. Franklin Roosevelt 50, 1050 Brussels, Belgium.*
[6] *Département de Géologie Générale, Centre de Recherches Géologiques et Minières, Democratic Republic of the Congo*

and basin evolution **([1 – 6])**. However, in deformed and metamorphosed belts, these primary volcanic features may be partly modified or obscured by recrystallization, sericitization, foliation development, quartz deformation and metamorphic mineral growth **([7 – 9])**. Distinguishing inherited volcanic textures from later tectono-metamorphic fabrics is therefore essential for interpreting mapped rhyolitic units and avoiding over-simplified reconstructions based only on lithological boundaries.

The West Congo Belt (WCB, Figures 1-2) preserves *a late Mesoproterozoic to Neoproterozoic* volcano-sedimentary succession along the western margin of the Congo Craton **([10])**. Its evolution involved extensional basin development, Tonian bimodal magmatism, and subsequent Pan-African deformation and metamorphism **([10 – 13])**. In the lower part of the West Congo Supergroup (Figure 2), the Seke-Banza Group includes rhyolites, subvolcanic microgranites and high-level granites, and tholeiitic basalts generally linked to intracontinental extension during the early stages of Rodinia breakup and West Congo basin development **([10], [12], [14], [15])**.

In the Tshela area of Kongo Central Province, the Lampa metarhyolites are represented on existing geological maps as part of the felsic Inga Formation (lower part of Seke-Banza Group) **([11], [16])**. Because descriptions of the petrochemical characteristics of the successive rhyolitic flows and of the Pan-African tectono-metamorphic overprint resulting in variably modified protoliths date from the late 1970-ies **([16], [17])**, they need urgent re-assessment. A more systematic study of the Lampa metarhyolites is thus essential for (i) an updated insight in their internal lithostratigraphic, petrochemical and radiometric characteristics, (ii) description of internal textural variability and (primary) volcanic features of the protolith, (iii) degree of modification by Pan-African deformation and regional metamorphism and eventual tectono-metamorphic gradient and (iv) geological and geodynamic significance and use in regional correlation within the West Congo Supergroup.

This study combines field observations, petrological study, and *in situ* LA-ICP-MS U-Pb titanite dating. The objectives are to document internal petrographic variabilities, distinguish preserved volcanic textures from secondary deformation-related fabrics, and evaluate whether the mapped rhyolitic unit is better interpreted as a homogeneous body or as a heterogeneous meta-rhyolitic architecture. U-Pb dating of titanite crystallization is used to constrain tectono-metamorphism, rather than the primary crystallization age of the rhyolitic protolith.

2. Regional Geology

The WCB (Figure 1) is a late Neoproterozoic to early Cambrian orogenic belt developed along the western margin of the Congo Craton during the Pan-African events. It preserves a nearly continuous record of the late Mesoproterozoic to Cambrian evolution of this margin, including intracontinental rifting associated with the initial breakup of Rodinia, Tonian bimodal magmatism, subsequent sedimentary basin development, and Pan-African deformation and metamorphism **([11], [12], [13], [18]).**

In the Kongo Central Province, this evolution is preserved within the West Congo Supergroup, which overlies the Paleoproterozoic Kimeza Supergroup **(**Figure 2**).** The Kimeza Supergroup consists predominantly of migmatitic paragneisses (dated at 2088 ± 91 Ma **([19], [20])**), orthogneisses, amphibolites, metaquartzites and subordinate marbles that underwent amphibolitic metamorphism at ca. 1.97 Ga **([21])**, together with locally exposed Mpozo syenomonzonite emplaced at ca. 1.97 Ga **([13])**. The overlying West Congo Supergroup records the transition from continental rifting to passive-margin sedimentation and comprises, from oldest to youngest, the Nzadi, the probably contemporaneous Seke-Banza and Tshela, and the Cataracts groups.

The Nzadi Group **(**Figure 2**)** represents the earliest preserved sedimentary succession of the basin and comprises the Matadi Formation (1126-1000 Ma), dominated by mature quartzites, and the overlying Yelala Formation (< 968 Ma), characterized by polymictic conglomerates interpreted as syn-rift deposits **([13])**.

This succession is followed by the Seke-Banza Group (*ca.* 920-900 Ma), which records widespread Tonian bimodal magmatism through the emplacement of continental tholeiitic flood basalts of the Gangila Formation overlain by a felsic volcano-plutonic complex including effusive and explosive rocks of the Inga Formation and –in the Lufu massif – associated prominent microgranites and high-level granites **([23])**. The Lampa metarhyolites are part of the Inga Formation **([10], [11], [16])**. The bimodal magmatism is widely interpreted as the endogenic expression of lithospheric extension during the early stages of Rodinia breakup **([10], [22])**.

According to the recent revision of the Kongo Central lithostratigraphy **([13])**, the Tonian lithostratigraphic succession comprises two laterally equivalent units, namely the Seke-Banza and Tshela groups **(**Figure 2**).** Although the depositional age of the volcano-sedimentary Tshela Group remains unconstrained, it is generally regarded as a lateral equivalent of the igneous Seke-Banza Group **([11], [13])**. It consists predominantly of (often) finely laminated dark metapelites, felsic and mafic metavolcanic rocks, presumably of explosive origin, dark metaquartzites, minor metabasalts, metaconglomerates and subordinate dolomitic lenses.

The succession is overlain by the Cataracts Group (*ca.* 900-541 Ma), composed of siliciclastic, diamictic and carbonate deposits **([24])**. The Lower Diamictite Subgroup including lenses of tholeiitic basaltic flows and subvolcanic feeder sills and dykes has been emplaced at *ca.* 694-678 Ma **([25 – 27])**.

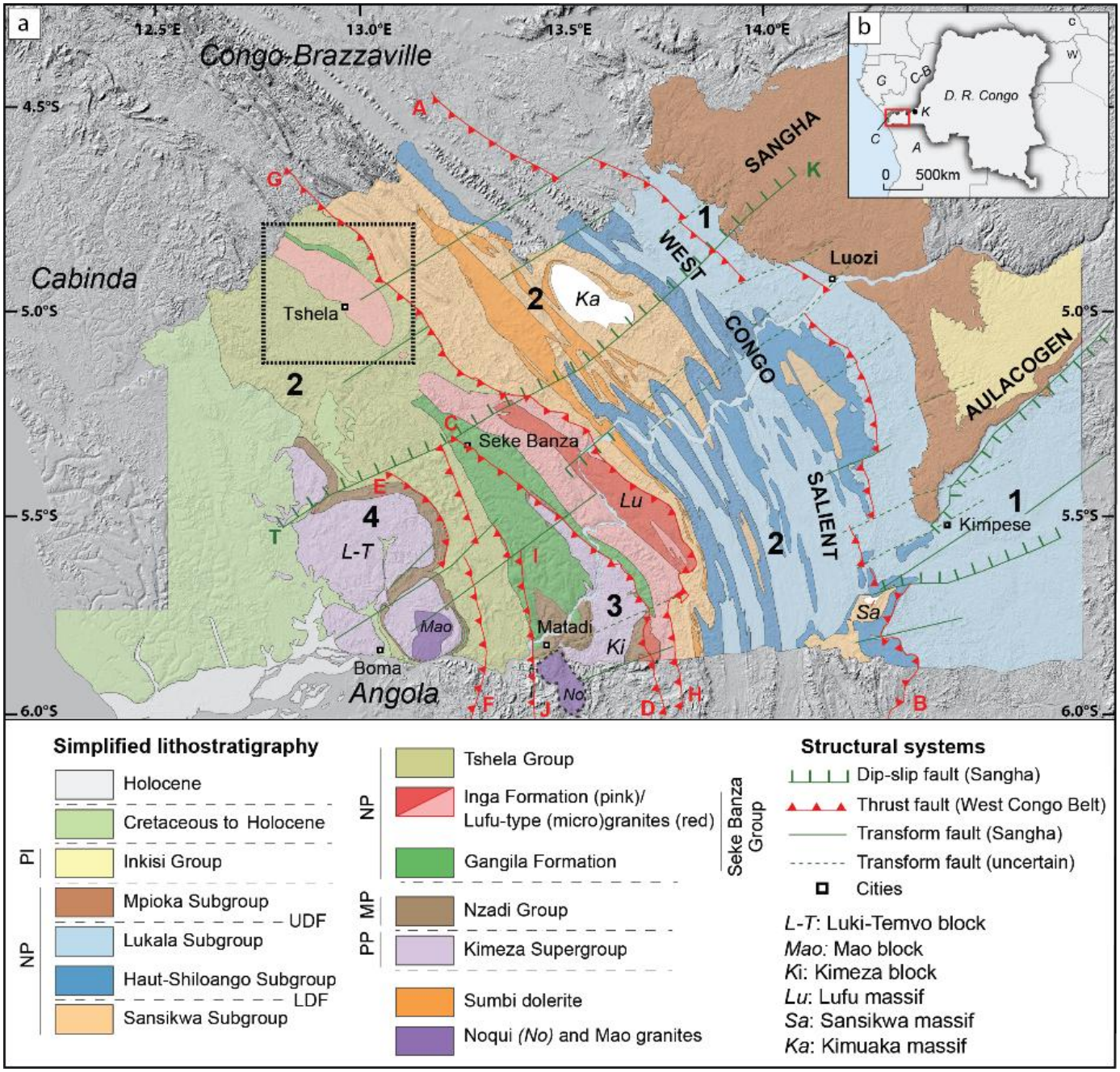


Figure 1: *(a) Regional geological map of the* ***West Congo Belt (WCB)*** *in* ***Kongo Central Province****, showing the main lithostratigraphic units, structural features, and four tectono-metamorphic domains: Domain 1: sedimentary to very low-grade; Domains 2–3: greenschist facies; and Domain 4: amphibolite facies. The* ***Tshela study area*** *is outlined by the black dashed rectangle. (b) Location of* ***Kongo Central Province*** *within the* ***DRC****:* ***G****, Gabon;* ***C-B****, Congo-Brazzaville;* ***C****, Cabinda;* ***A****, Angola;* ***K****, Kinshasa. (c) Schematic W–E section showing the regional metamorphic zonation across the WCB. Modified after* **([28], [11])**.

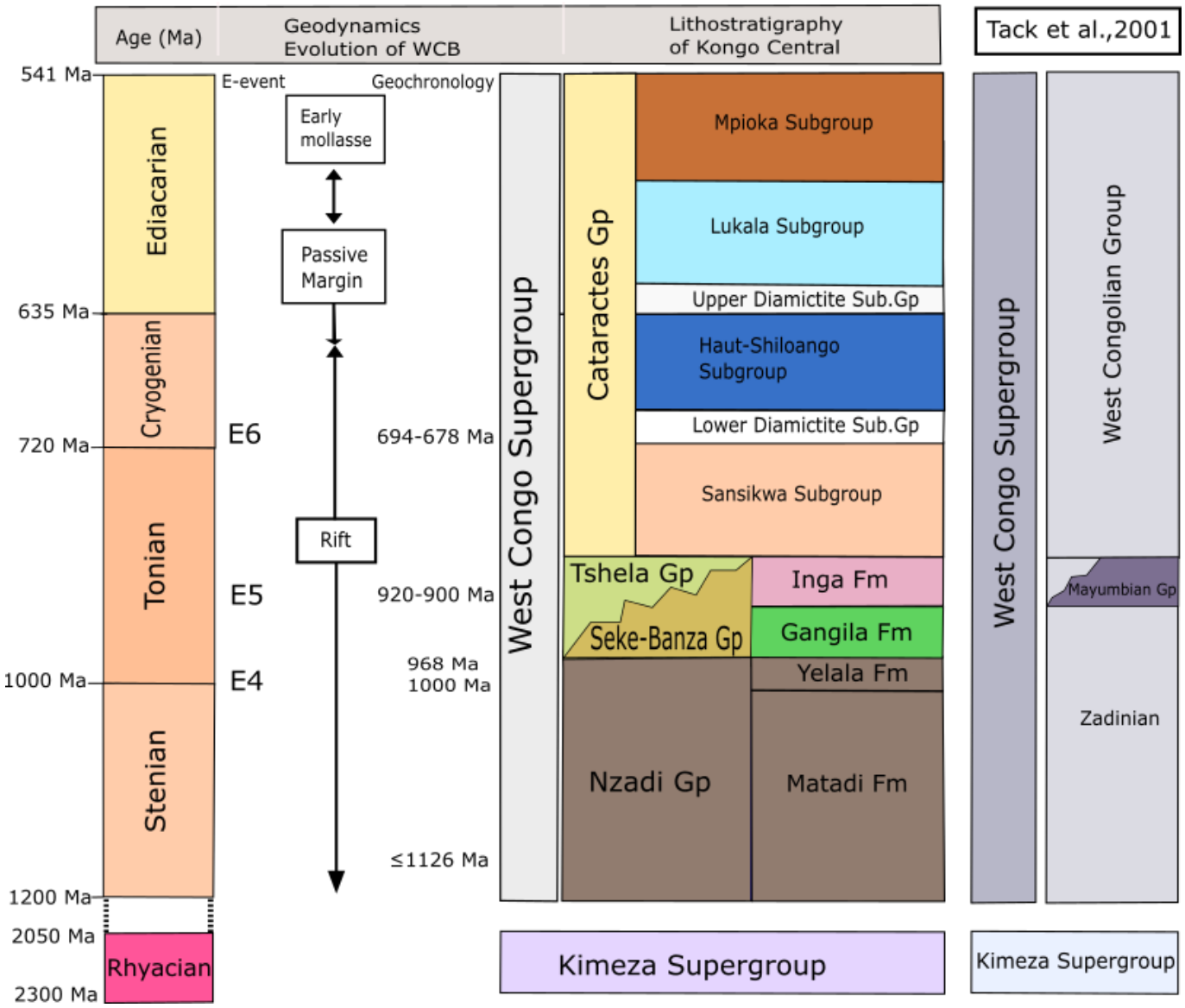


Figure 2*: Updated lithostratigraphic framework of the* ***West Congo Supergroup*** *in the* ***Kongo Central Province****, showing the revised litho-chronostratigraphic relationships between the* ***Nzadi, Seke-Banza, Tshela,*** *and* ***Cataracts*** *groups, together with the geodynamic evolution of the West Congo Belt (WCB) Modified from (***[13]).**

3. Materials and Methods

3.1 Fieldwork

Field investigations were conducted in February 2025, in the Tshela area, Kongo Central Province, with the aim of documenting the distribution, field relationships and textural variability of the Lampa metarhyolites The field campaign was guided by published (**[16], [17]**), and unpublished geological data compiled at the Royal Museum for Central Africa (Tervuren), Belgium, and academic datasets from University of Kinshasa (D.R Congo).

The present study focuses on six representative samples (TSH-25-03, TSH-25-15, TSH-25-43, TSH-25-54, TSH-25-56, and TSH-25-63**;** Figure 3).

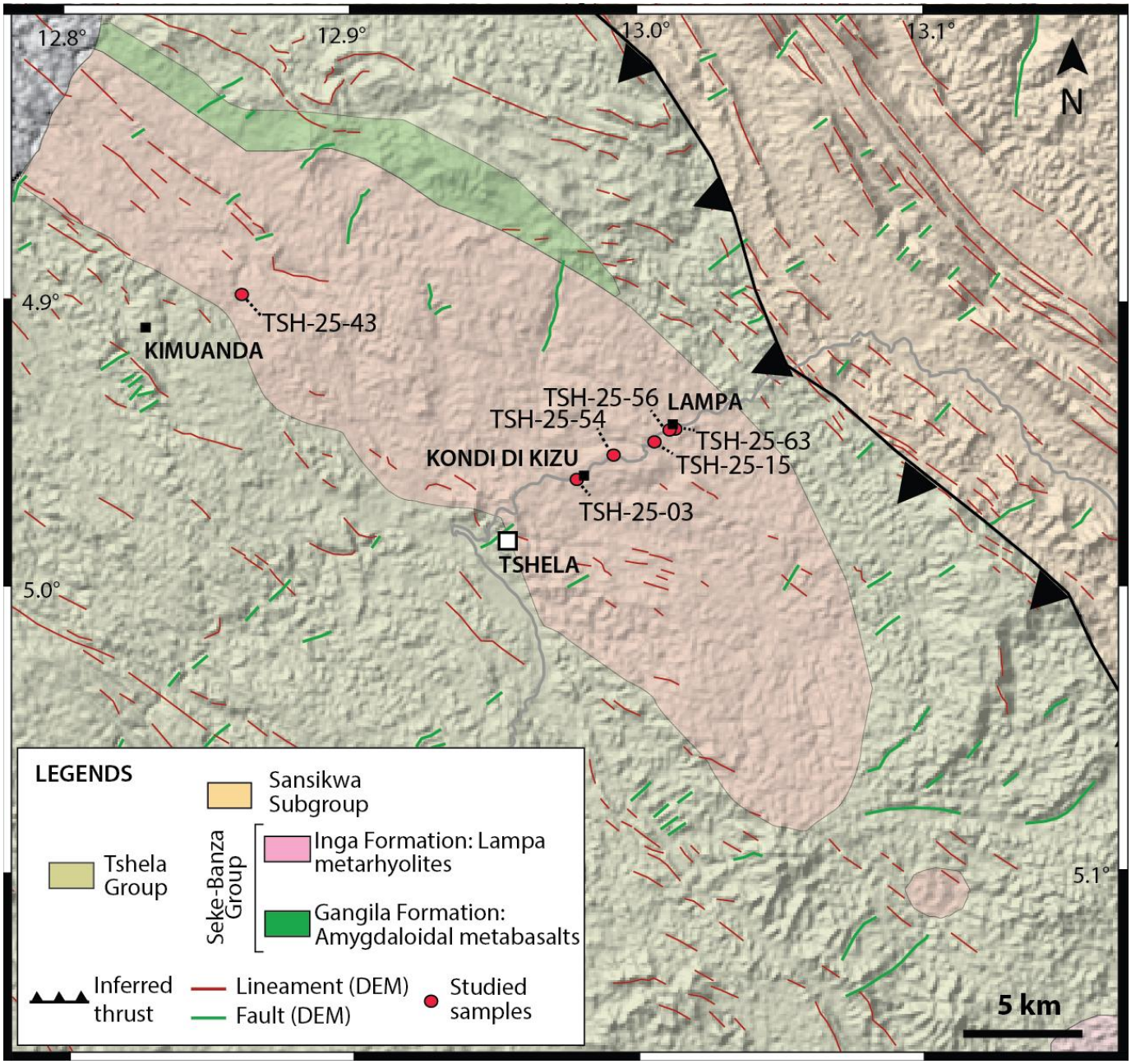


Figure 3**: Geological map of the **Tshela studied area**, showing the distribution of the representative samples analyzed in this study. **Modified from ([11],[16]). The faults and lineaments are interpretative and derived from the DEM analysis (TPI layer and MDOW hillshade).

3.2 Petrographic Analysis

Polished thin sections were prepared from representative samples at KU Leuven, Belgium. Petrographic observations were carried out using a Leica DMP4 polarizing microscope under plane-polarized light and cross-polarized light, with ×2.5, ×5 and ×10 objectives. Microphotographs were acquired using a Leica Flexacam C3 camera and LAS X software.

The petrographic description focused on features relevant to reconstructing the internal architecture and post-emplacement modification of the Lampa metarhyolites. Particular attention was given to primary and/or recrystallization features of the matrix, matrix/crystal ratio, quartz and feldspar abundance, phenocryst morphology and preservation, sericitization, quartz deformation textures, foliation intensity, occurrence of crenulation cleavage, and the distribution of secondary (recrystallization) minerals. These criteria were used to distinguish relict primary volcanic textures of the protolith from later deformation-related and metamorphic fabrics.

3.3 Scanning Electron Microprobe

Scanning electron microscopy (SEM) was used to characterize mineral assemblages and microtextural relationships in one selected Lampa metarhyolite sample. Analyses were performed on 10-20 nm carbon-coated polished thin sections using a SNE-4500M Plus (NanoImages, Canada) at the Laboratoire G-Time (Université Libre de Bruxelles, Belgium), under backscattered electron (BSE) view, with an acceleration

voltage of 15 kV and a beam intensity of 110 µA. The SEM is coupled to a Bruker XFlash® energy-dispersive X-ray spectroscopy (EDS) detector with a QUANTAX system (Bruker S.A.). Backscattered-electron (BSE) imaging was employed to investigate mineral textures and compositional contrasts, while EDS supported mineral identification and the recognition of phases not readily distinguished by optical microscopy. Observations focused on quartz, feldspar, biotite, titanite, Fe-Ti oxides, apatite and other accessory minerals within the recrystallized matrix and deformation-related fabrics. Particular attention was given to the occurrence and textural setting of titanite in relation to Fe-Ti oxides and matrix recrystallization domains to assess whether it represents a primary magmatic phase or a secondary mineral formed during metamorphism and/or fluid-assisted alteration.

3.4 LA-ICP-MS U-Pb titanite geochronology

U-Pb analyses were performed on titanite grains directly in polished thin sections and mount of selected metarhyolite samples TSH-25-03 and TSH-25-15 at the GeOHeLiS analytical platform, Université de Rennes (France). Analyses were carried out using a 193 nm Excimer laser ablation system (ESI NWR193UC) coupled to an Agilent 7850 ICP-MS. Analytical conditions included a beam diameter of 40 µm and a repetition rate of 5 Hz.

The ablated material was transported in a helium carrier gas (0.76 L/min) and mixed with nitrogen (0.06 L/min) and argon (0.47 L/min) prior to introduction into the plasma source. The isotopes ^{204}(Pb + Hg), ^{206}Pb, ^{207}Pb, ^{208}Pb, ^{232}Th, and ^{238}U were measured during each analysis. The abundance of ^{235}U was calculated from ^{238}U using a fixed ^{238}U/^{235}U ratio of 137.818. Each analytical cycle consisted of approximately 20 s of background acquisition, 40 s of laser ablation, and 10 s of washout.

Data reduction was carried out using the Iolite in time-resolved mode **([29])**. Raw data were corrected for laser-induced elemental fractionation (Pb/U and Pb/Th) and instrumental mass bias using the standard-sample bracketing approach. The OLT1 titanite reference material **([30])** was used for calibration. The McClure titanite standard (523.3 ± 1.3 Ma; **([31])**) was analyzed as an independent monitor of analytical accuracy and precision and yielded an age of 515 ± 36 Ma (n = 3), consistent within uncertainty with the published reference value.

4. Results

4.1. Field characteristics of the Lampa metarhyolites

The Lampa metarhyolitic rocks are exposed at several localities in the Tshela area, including Kimakonga, Kondi di Kizu, Nzamba-Zunga, the Tadi River area and the eastern margin of the study area (Figure 3). In the field, they occur as homogeneous, grey to dark grey rocks characterized by conspicuous bluish quartz and feldspar crystals enclosed within a fine-grained matrix. The relative abundance and distribution of these phenocrysts vary among the studied samples, defining a continuum from matrix-rich facies with dispersed, separate, individual quartz and/or feldspar phenocrysts to crystal-rich facies containing a higher proportion of phenocrysts. Sample TSH-25-43 is more heterogeneous and strongly crenulated and is described separately based on its petrographic features.

The studied metarhyolites exhibit variable degrees of deformation, ranging from massive to weakly and locally strongly foliated. A planar fabric is weakly developed in sample TSH-25-03 from Kondi di Kizu area, but becomes progressively more pronounced in samples TSH-25-15, TSH-25-54, TSH-25-56 and TSH-25-63. Near Lampa, sample TSH-25-56 exhibits a well-developed foliation associated with local crenulation structures. These field observations provide the framework for the petrographic descriptions presented in the following sections.

4.2. Relict volcanic (effusive and explosive) facies of the Lampa metarhyolites

Petrographic observations show that the Lampa metarhyolitic rocks preserve relict volcanic features despite subsequent tectono-metamorphic modification. Based on the relative abundance of the felsic matrix and quartz-feldspar phenocrysts, three volcanic facies (protoliths) are recognized: **(i)** effusive matrix-rich metarhyolites, **(ii)** effusive crystal-rich metarhyolites, and **(iii)** explosive facies.

The matrix-rich facies, represented by samples TSH-25-03, TSH-25-54 and TSH-25-56, is characterized by a predominance of fine-grained felsic matrix enclosing dispersed quartz and feldspar phenocrysts (Figures 4, 5 & 6). Quartz commonly occurs as subhedral to subrounded crystals, whereas feldspar forms subhedral to anhedral phenocrysts that generally retain their primary crystal outlines despite variable alteration. The relatively low phenocryst abundance and their homogeneous distribution impart a weakly porphyritic texture.

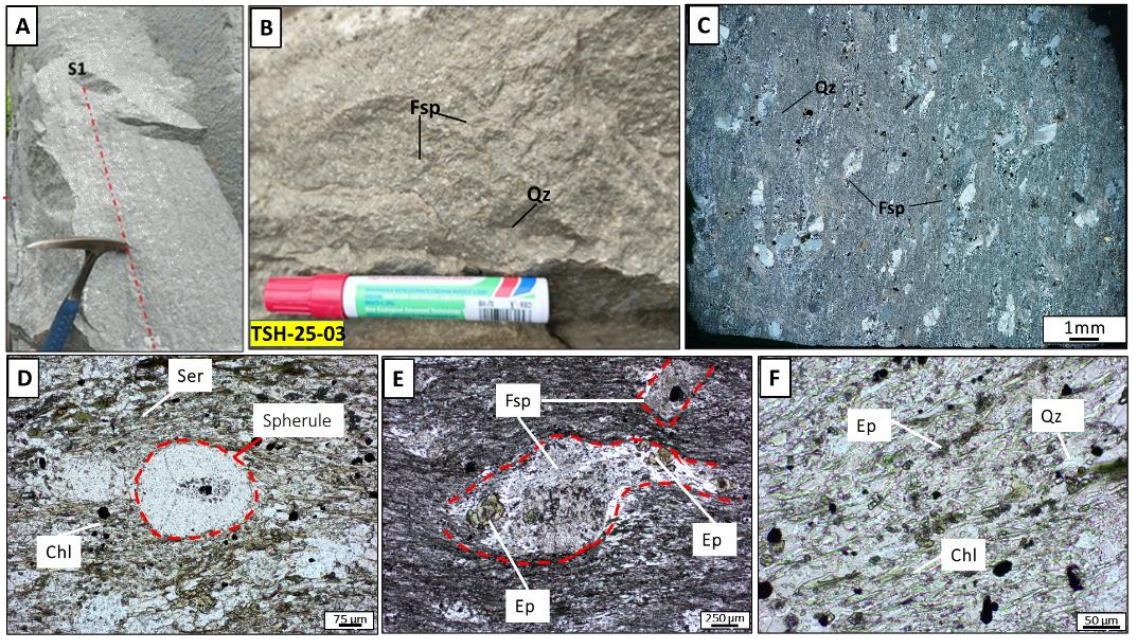


Figure 4: *Field occurrence and petrographic characteristics of the Kondi di Kizu metarhyolite (TSH-25-03).* ***(A)*** *Outcrop view showing a massive to weakly foliated facies; the red dashed line indicates the orientation of foliation.* ***(B)*** *Hand specimen displaying quartz (Qz) and feldspar (Fsp) phenocrysts within a fine-grained felsic matrix.* ***(C)*** *Thin-section photomicrograph under crossed-polarized light (XPL) showing a porphyritic texture with quartz and feldspar phenocrysts embedded in a fine recrystallized matrix.* ***(D)*** *PPL photomicrograph illustrating a spherulitic texture (Spherule) surrounded by a chlorite-rich matrix (Chl), with associated sericite (Ser), suggesting devitrification of an original felsic volcanic material.* ***(E)*** *Plane-polarized light (PPL) image showing altered feldspar (Fsp) crystals enclosed in a foliated matrix rich in epidote (Ep), indicative of metamorphic and hydrothermal alteration.* ***(F)*** *PPL photomicrograph showing chlorite (Chl), epidote (Ep), and quartz (Qz) aligned within the schistose matrix, reflecting low-grade metamorphic overprint and hydrothermal recrystallization.*

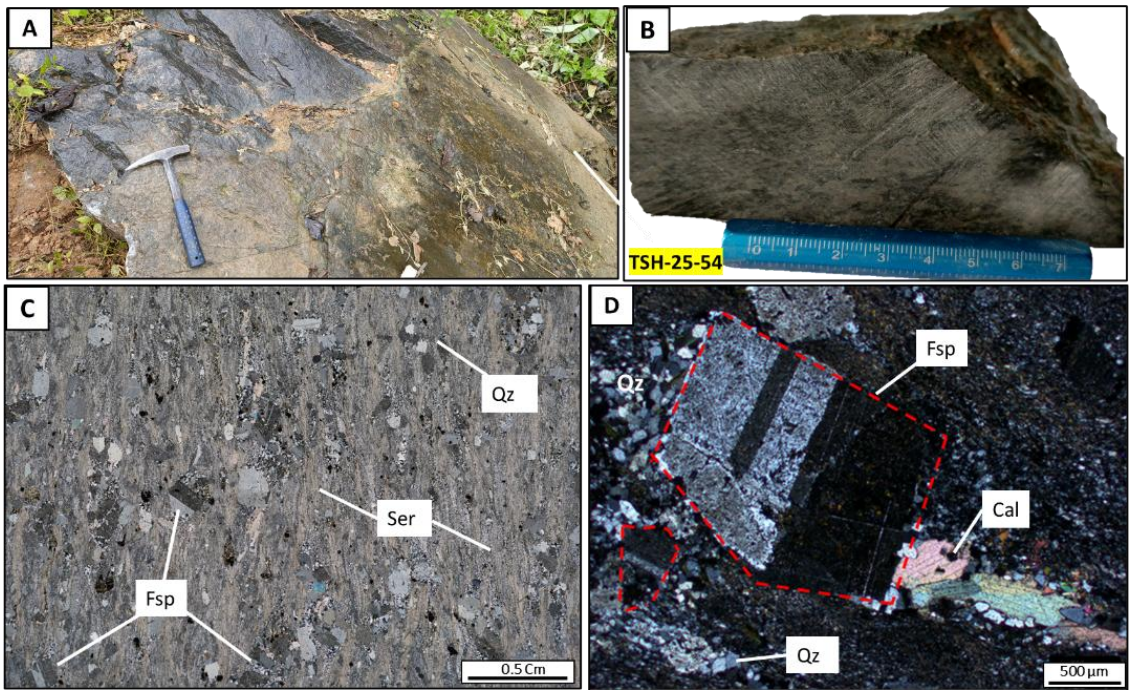


Figure 5*: Field and petrographic characteristics of metarhyolite sample TSH-25-54 from Nzamba-Zunga village.* ***(A)*** *Field exposure of a dark grey, fine-grained metarhyolite displaying an apparently massive aspect and irregular fractures.* ***(B)*** *Hand specimen of TSH-25-54 showing a dark grey, fine-grained and macroscopically homogeneous rock.* ***(C)*** *Plane-polarized light (PPL) photomicrograph showing quartz (Qz) and feldspar crystals (Fsp) dispersed within a fine-grained sericite-bearing matrix (Ser), in which a preferential mineral alignment is locally visible.* ***(D)*** *Cross-polarized light (XPL) photomicrograph showing a partially altered feldspar crystal (Fsp), outlined by the red dashed line, within a fine-grained quartz-rich matrix (Qz). Calcite (Cal) occurs locally adjacent to the feldspar.*

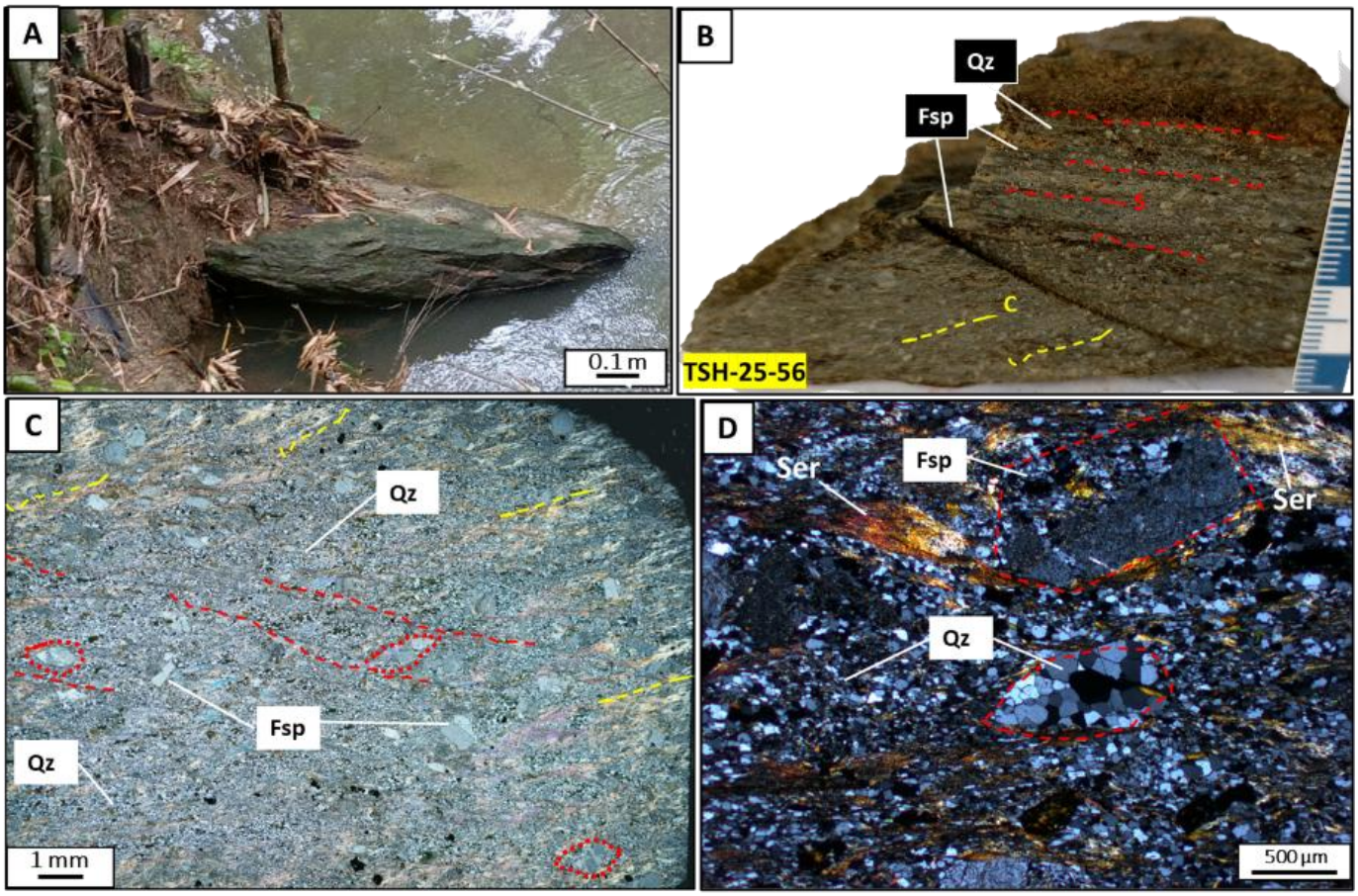


Figure 6: *Field and petrographic characteristics of metarhyolite sample TSH-25-56 from the Tadi River area.* ***(A)*** *Outcrop view showing a weakly developed planar fabric.* ***(B)*** *Hand specimen displaying quartz (Qz) and feldspar (Fsp) crystals within a fine-grained felsic matrix. The main foliation (S) is outlined by red dashed lines, whereas yellow dashed lines indicate crenulation structures(C).* ***(C)*** *Thin-section photomicrograph (XPL) showing a foliated matrix composed of quartz (Qtz), feldspar (Fsp),.* ***(D)*** *Enlarged XPL view showing partially recrystallized feldspar (Fsp) and quartz (Qz) phenocrysts enclosed within a sericite-rich foliated matrix (Ser).*

The crystal-rich facies, represented by samples TSH-25-15 and TSH-25-63, contains a markedly higher proportion of quartz and feldspar phenocrysts relative to the matrix (Figures 7 & 8). Quartz phenocrysts are typically subhedral to rounded and occur either as isolated crystals or locally as small crystal aggregates, whereas feldspar phenocrysts are abundant throughout the rock. Compared with the matrix-rich facies, the higher phenocryst content produces a more distinctly porphyritic texture.

In sample TSH-25-15, the assemblage includes quartz, feldspar (K-feldspar and albite), biotite, epidote, sericite, titanite, Mn-rich ilmenite and apatite (Figure 7). Titanite occurs as small anhedral grains and locally in close spatial association with Fe-Ti oxides (Figure 7E). Biotite is present in the recrystallized matrix, whereas apatite occurs as small accessory grains.

The textural relationship between titanite and Fe-Ti phases is important because titanite is not observed as large euhedral phenocrysts. Instead, it occurs as fine grains or reaction-related phases within recrystallized domains.

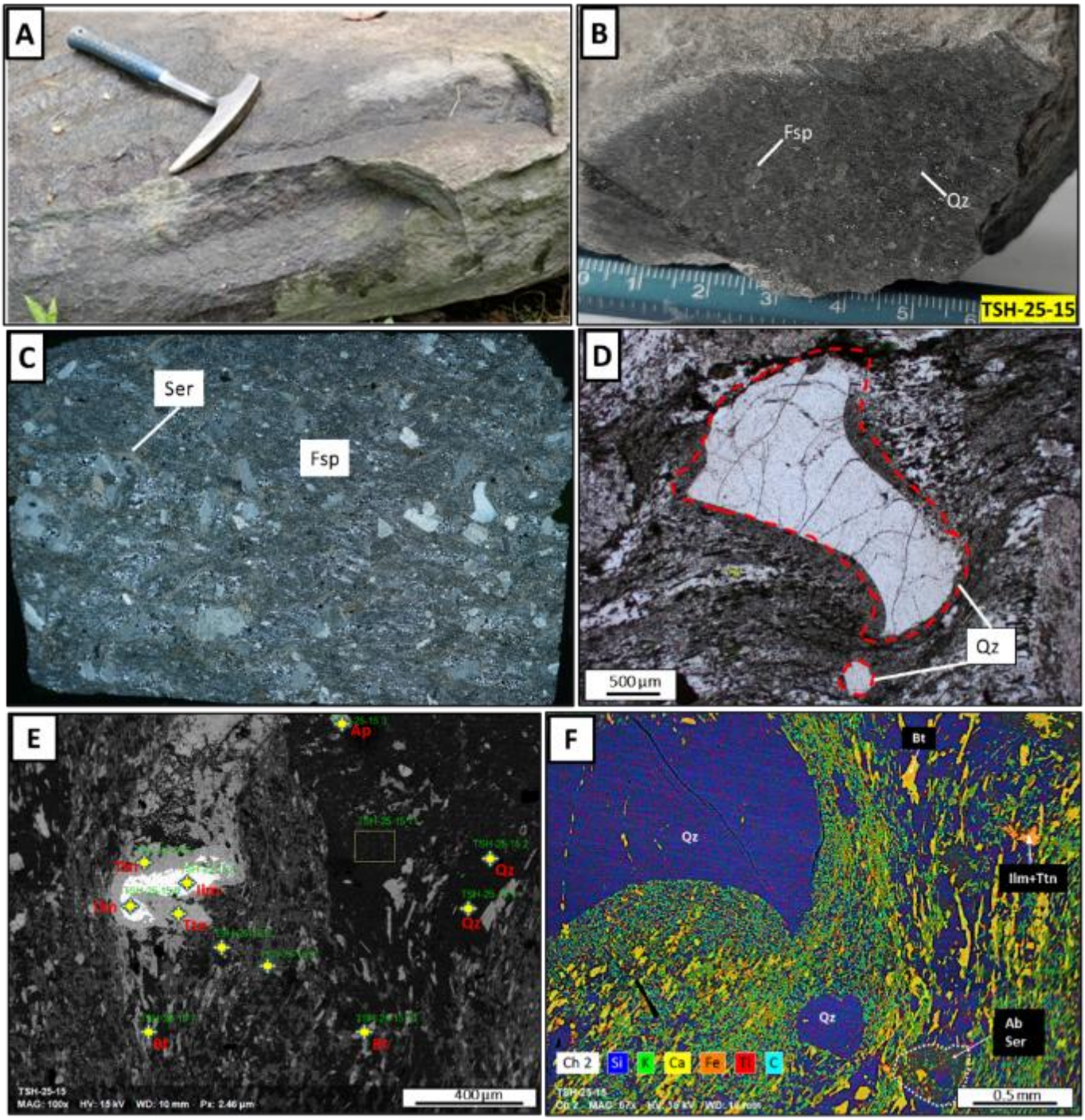


Figure 7: *Field, petrographic, and SEM characteristics of the metarhyolite sample TSH-25-15.* ***(A)*** *Outcrop view.* ***(B)*** *Hand specimen showing quartz (Qz) and feldspar (Fsp) phenocrysts in a fine-grained felsic groundmass.* ***(C)*** *Thin-section photomicrograph (XPL) illustrating the porphyritic and/or glomeroporphyritic texture with feldspar (Fsp), quartz (Qz), and a sericitized matrix (Ser).* ***(D)*** *Enlarged PPL view of a "rhyolitic" quartz phenocryst (Qz) (fragmentation cracks, corroded with sharp or curved edges) outlined by dashed red lines.* ***(E)*** *BSE image showing quartz (Qz), biotite (Bt), titanite (Ttn), ilmenite (Ilm), and apatite (Ap).* ***(F)*** *SEM-EDS elemental map (Si-K-Ca-Fe-Ti-C). Abbreviations: Qz = quartz; seric = sericite; Ab: albite; Bt = biotite; Ttn= titanite; Ilm = ilmenite.*

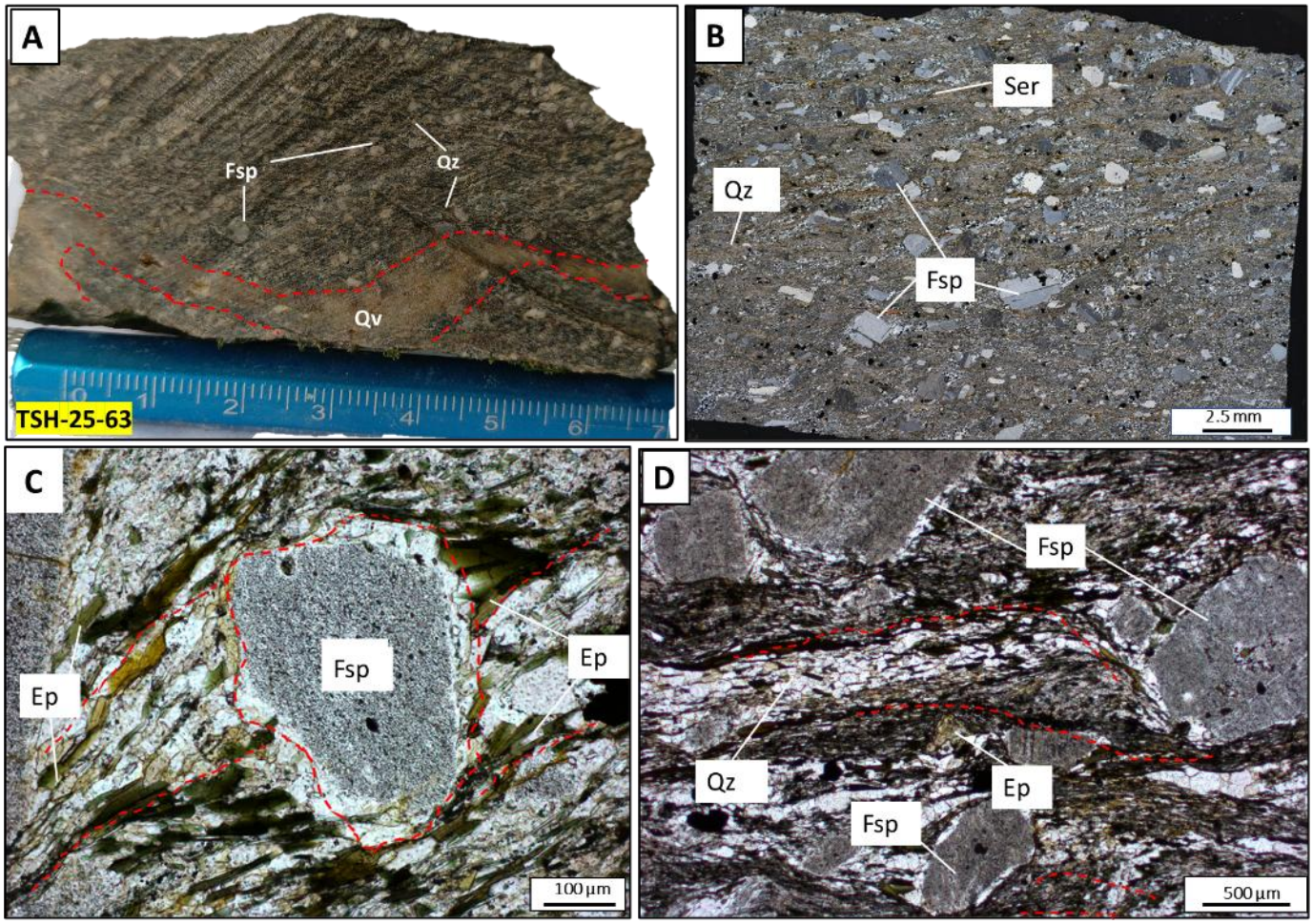


Figure 8. *Macroscopic and petrographic characteristics of the crystal-rich metarhyolite sample TSH-25-63. (A) Hand specimen showing quartz (Qz) and feldspar (Fsp) crystals in a foliated matrix crosscut by a quartz vein (Qv). (B) Thin-section overview showing abundant quartz (Qz) and feldspar (Fsp) crystals within a sericite-rich (Ser) foliated matrix. (C) PPL photomicrograph showing a feldspar porphyroclast (Fsp) wrapped by an epidote-bearing (Ep) foliated matrix. (D) PPL photomicrograph showing a porphyroclastic fabric defined by quartz (Qz) and feldspar (Fsp) porphyroclasts within an epidote-bearing foliated matrix.*

The explosive facies (tuff)

The hand specimen sample TSH-25-43 displays a well-developed foliation affected by strong crenulation cleavage giving rise to well-expressed individual microlithons (Figure 9A). In addition to the strong tectonic overprint, the recrystallized matrix is dominated by prominent aligned chlorite-rich phyllosilicates defining a pervasive foliation wrapping around large subhedral to anhedral quartz crystals, producing a well-developed porphyroclastic fabric. The polished thin section (Figure 9B) reveals a relatively heterogeneous rock containing scattered quartz phenocrysts and a preferential original linear alignment of opaques, now interrupted and displaced because of the microlithon fabric. Under plane-polarized light (Figures 9C-E), distinctive volcanic relict features subsist, including “rhyolitic” amoeboid and embayed quartz phenocrysts with internal cracks and phenocryst fragments, locally preserved volcanic glass, and aligned possible glass shards. Within each microlithon, the preferential alternation of the recrystallized phyllosilicates, grey quartz-feldspar mini-layers and/or variation in abundance of opaques marks an internal compositional layering of the rock. These features suggest that the protolith resulted from explosive tuffaceous rather than effusive volcanism. Although previously unobserved in the Lampa area the occurrence of tuffs is not surprising as they are well-known in the Inga area **([17])**.

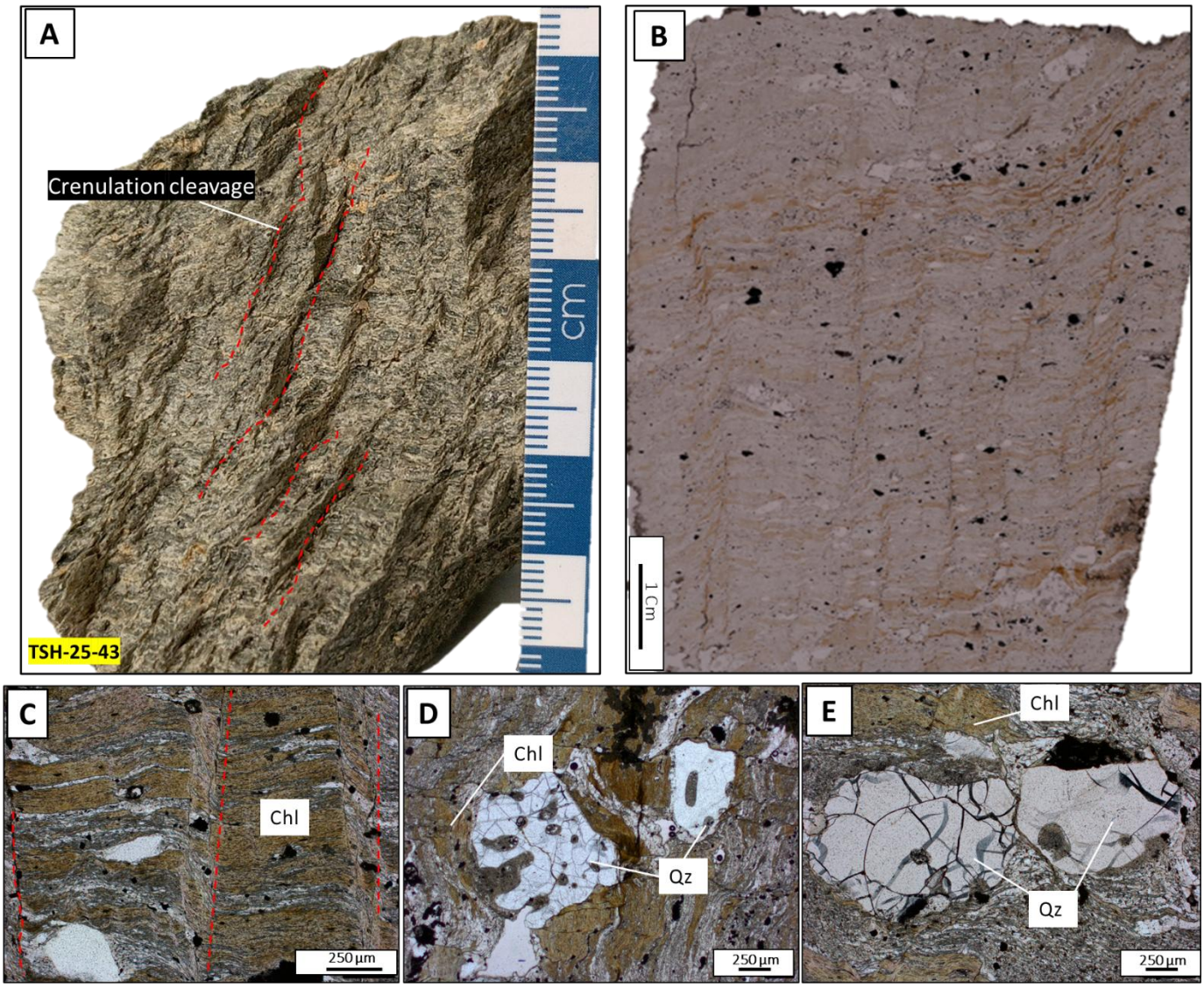


***Figure 9**: Petrographic characteristics of metarhyolitic tuff sample **TSH-25-43**. **(A)** Hand specimen showing a well-developed foliation locally affected by crenulation cleavage (red dashed lines). **(B)** PPL whole-thin-section scan showing the heterogeneous distribution of quartz (Qz) crystals within a fine-grained felsic matrix and the preferential alignment of opaque minerals. **(C)** PPL photomicrograph showing a matrix dominated by strongly aligned chlorite-rich phyllosilicates (Chl), alternating with grey quartz-feldspar-rich mini-layers (red dashed lines), defining an internal compositional layering. **(D)** PPL image illustrating fractured and embayed quartz (Qz) crystals enclosed within the foliated chlorite-rich (Chl) matrix. The lower right part of the image preserves aligned flattened shard-like relics associated with a preferential concentration of opaque minerals, suggesting relict primary volcanic layering. **(E)** PPL photomicrograph showing a well-developed porphyroclastic fabric, with the foliated matrix wrapping around fractured quartz crystals.*

4.3. U-Pb dating on titanite

In situ Titanite U-Pb analyses were obtained from metarhyolite samples TSH-25-03 and TSH-25-15. Representative titanite grains analyzed by LA-ICP-MS are shown in (Figure 10).

In sample TSH-25-03, titanites occur as subhedral to anhedral grains dispersed within the metarhyolitic matrix (Figures. 10A-B). A total of 20 *in situ* analyses were performed on titanite grains in thin section, of which 17 were retained for age calculation (Table 1). The analyzed titanites contain between 4 and 109 ppm U and 981 to 20,636 ppm Pb, with Th/U ratios ranging from 0.09 to 1.04 (Table 1). The retained analyses (n = 17) define a coherent array on the Tera-Wasserburg diagram and yield a lower-intercept age of 540 ± 32 Ma, with a MSWD of 1.5 (Figure 11A).

In sample TSH-25-15, titanites form reaction rims and external overgrowths around ilmenite (Figures

10C-D). A total of 60 *in situ* titanite analyses were carried out on both thin section and grain mounts, of which 55 were retained for age calculation. These titanites contain between 0.4 and 64 ppm U and 206 to 9,532 ppm Pb, with Th/U ratios ranging from 0.0004 to 4.42 (Table 1). The retained analyses (n = 55) define a well-constrained regression on the Tera-Wasserburg diagram and yield a lower-intercept age of 560.2 ± 15.3 Ma, with a MSWD of 2.7 (Figure 11B).

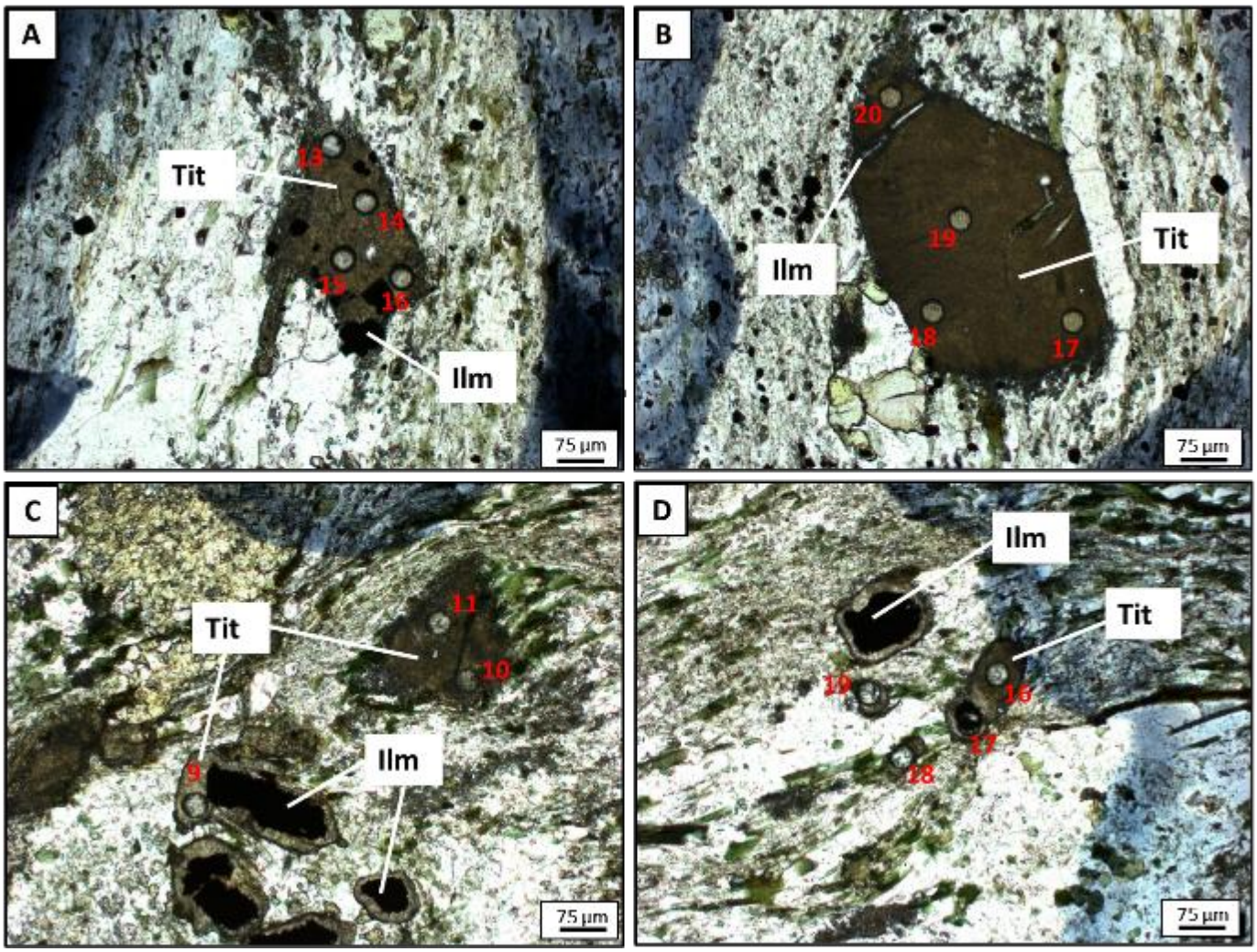


***Figure 10**: Representative titanite grains dated by U-Pb geochronology in thin sections from samples TSH-25-03 and TSH-25-15, showing the locations of the LA-ICP-MS analysis spots. **(A-B)** Subhedral to anhedral titanite grains from sample TSH-25-03; **(C-D)** titanites form reaction rims and external overgrowths around ilmenite from sample TSH-25-15. All images were acquired under plane-polarized light (PPL).*

Table 1: LA-ICP-MS U-Pb analytical data for titanite from metarhyolite samples TSH-25-03 and TSH-25-15, including Tera-Wasserburg and Wetherill concordia age calculations.

	22 April 2026, GeOHeLiS Platform, Universite Rennes				**Data for Tera-Wasserburg plot**					**Data for Wetherill plot**				
	Identifier	Uppm	Th/U	Pbppm	238U/206Pb	2se%	207Pb/206Pb	2se%	rho	207Pb/235U	2se%	206Pb/238U	2se%	Rho
TSH-25-15.01	Mount	2.1	0.19	2478.3	1.05	5.4	0.75096	3.0	0.31	97.9325	5.1	0.95367	5.4	0.84
TSH-25-15.02	Mount	3.6	0.13	1620.0	2.04	5.6	0.66512	2.5	-0.31	45.9413	6.1	0.49053	5.6	0.92
TSH-25-15.03	Mount	4.3	0.22	4073.2	1.23	3.7	0.71981	2.4	0.48	79.5142	2.9	0.81116	3.7	0.73
TSH-25-15.04	Mount	1.8	0.21	1004.1	1.73	2.9	0.71808	2.5	0.52	55.9140	2.6	0.57729	2.9	0.53
TSH-25-15.05	Mount	2.9	3.67	1387.1	1.89	3.4	0.70873	3.0	0.54	51.4299	3.1	0.52994	3.4	0.56
TSH-25-15.06	Mount	2.0	0.11	818.9	1.73	2.7	0.71066	1.9	0.46	56.1978	2.4	0.57918	2.7	0.62
TSH-25-15.07	Mount	2.2	0.21	869.7	1.78	2.7	0.71185	2.0	0.30	54.9692	2.6	0.56231	2.7	0.66
TSH-25-15.08	Mount	2.1	0.16	864.8	1.56	2.9	0.72630	2.5	0.61	63.3520	2.5	0.63931	2.9	0.50
TSH-25-15.09	Mount	2.2	0.11	748.6	1.66	2.9	0.72611	1.8	0.17	60.1840	2.9	0.60403	2.9	0.76
TSH-25-15.10	Mount	2.5	0.09	731.4	1.77	5.8	0.69160	3.1	0.11	53.1489	5.8	0.56389	5.8	0.83
TSH-25-15.11	Mount	2.9	0.28	848.1	1.87	2.4	0.70816	1.8	0.55	51.7740	2.0	0.53419	2.4	0.53
TSH-25-15.12	Mount	2.3	0.16	849.7	1.57	2.6	0.72490	1.7	0.41	63.0402	2.2	0.63711	2.6	0.67
TSH-25-15.13	Mount	2.7	0.15	787.5	1.80	3.0	0.69021	1.8	0.09	52.5573	2.9	0.55508	3.0	0.77
TSH-25-15.14	Mount	2.8	0.25	796.9	2.01	2.4	0.67982	2.0	0.51	46.3384	2.2	0.49871	2.4	0.52
TSH-25-15.15	Mount	2.4	0.15	868.8	1.71	2.8	0.72049	1.9	0.41	57.4100	2.5	0.58495	2.8	0.66
TSH-25-15.16	Mount	3.5	0.61	814.0	2.65	3.9	0.64105	2.4	0.22	33.0660	4.0	0.37713	3.9	0.79
TSH-25-15.17	Mount	6.9	4.42	2059.6	2.09	2.0	0.67918	1.2	0.38	44.5846	1.7	0.47956	2.0	0.66
TSH-25-15.18	Mount	2.1	1.29	851.4	1.64	4.0	0.71286	3.8	0.53	58.4778	3.7	0.60947	4.0	0.53
TSH-25-15.19	Mount	2.2	0.82	1114.9	1.32	2.4	0.73173	1.8	0.40	76.4244	2.3	0.75860	2.4	0.60
TSH-25-15.20	Mount	1.9	0.94	678.1	1.83	3.3	0.67131	3.7	0.46	49.8325	3.3	0.54792	3.3	0.39
TSH-25-15.21	Mount	2.1	0.05	568.4	1.74	4.3	0.70100	3.7	0.56	54.2044	3.5	0.57406	4.3	0.55
TSH-25-15.22	Mount	2.6	0.07	648.0	2.00	2.9	0.68825	2.1	0.45	47.2308	2.6	0.49998	2.9	0.65
TSH-25-15.23	Mount	2.4	0.11	1045.1	1.24	3.4	0.73978	2.1	0.27	82.4013	3.8	0.80366	3.4	0.81
TSH-25-15.24	Mount	2.6	0.10	1049.8	1.34	4.8	0.73839	3.7	0.43	75.3254	4.6	0.74674	4.8	0.70
TSH-25-15.25	Mount	1.7	0.22	488.4	1.86	5.8	0.65665	4.7	0.55	47.6210	5.1	0.53716	5.8	0.61
TSH-25-15.26	Mount	2.3	0.34	576.9	2.18	4.8	0.66236	3.7	0.38	41.4955	4.4	0.45821	4.8	0.62
TSH-25-15.27	Mount	2.3	0.45	777.6	1.73	3.2	0.69234	2.7	0.42	54.7719	3.0	0.57889	3.2	0.59
TSH-25-15.28	Mount	3.8	0.00	250.9	5.13	3.0	0.48516	3.0	0.50	12.7420	2.9	0.19499	3.0	0.46
TSH-25-15.29	Mount	3.6	0.03	254.6	4.84	2.8	0.48438	2.8	0.55	13.4535	2.8	0.20643	2.8	0.40
TSH-25-15.30	Mount	1.7	0.00	213.7	3.27	4.2	0.60655	4.6	0.52	24.5932	4.3	0.30585	4.2	0.41
TSH-25-15.31	Mount	0.4	0.00	205.8	1.08	4.1	0.75563	3.4	0.59	95.0772	3.7	0.92672	4.1	0.53
TSH-25-15.32	Mount	0.4	0.00	221.3	1.05	5.0	0.77705	4.4	0.62	98.0469	4.4	0.95070	5.0	0.61
TSH-25-15.33	Mount	21.8	0.01	571.5	7.64	2.3	0.31040	2.2	0.49	5.5326	2.2	0.13083	2.3	0.38
TSH-25-15.34	Mount	14.3	0.01	363.0	7.72	2.1	0.30070	2.3	0.48	5.3193	2.3	0.12951	2.1	0.27
TSH-25-15.35	Mount	13.4	0.01	609.6	6.23	3.5	0.41439	3.2	0.30	9.2414	4.1	0.16060	3.5	0.58
TSH-25-15.36	Mount	14.2	0.01	1182.7	4.52	3.4	0.52136	2.1	0.16	15.9518	3.6	0.22131	3.4	0.80
TSH-25-15.37	Mount	10.1	0.01	367.4	6.53	3.9	0.35744	4.0	0.58	7.3807	3.6	0.15325	3.9	0.35
TSH-25-15.38	Mount	1.0	0.00	326.4	1.51	4.3	0.70817	3.3	0.51	62.1716	4.0	0.66195	4.3	0.64
TSH-25-15.39	Mount	2.2	0.16	875.6	1.45	3.6	0.70043	2.7	0.55	65.4920	2.9	0.69199	3.6	0.63
TSH-25-15.40	Mount	3.2	0.20	613.1	2.46	7.5	0.65578	3.9	0.25	36.4617	7.4	0.40689	7.5	0.84
TSH-25-15.03	Thin section	2.9	0.6	1199.8	1.04	6.3	0.76790	1.8	0.38	101.1609	7.4	0.96478	6.3	0.74
TSH-25-15.04	Thin section	10.4	0.4	6532.5	0.75	6.6	0.80964	1.7	0.30	147.8571	7.7	1.33750	6.6	0.87
TSH-25-15.05	Thin section	4.1	1.0	2237.5	0.87	7.5	0.78969	2.4	0.28	126.3053	8.6	1.14969	7.5	0.90
TSH-25-15.06	Thin section	3.4	0.2	2147.8	0.82	6.1	0.78931	1.4	0.31	132.5177	7.3	1.22074	6.1	0.82
TSH-25-15.07	Thin section	2.4	0.9	1787.3	0.76	6.9	0.80428	2.7	0.32	146.0458	8.1	1.32099	6.9	0.79
TSH-25-15.09	Thin section	5.1	0.8	3635.6	0.84	7.3	0.79300	1.7	0.11	129.2533	8.4	1.18688	7.3	0.91
TSH-25-15.11	Thin section	2.0	0.5	1143.5	0.96	6.3	0.77158	2.1	0.31	109.4006	7.4	1.03879	6.3	0.63
TSH-25-15.12	Thin section	2.1	0.4	1651.2	0.72	6.2	0.79873	1.6	0.30	152.4460	7.3	1.39744	6.2	0.77
TSH-25-15.13	Thin section	1.2	0.0	1044.2	0.65	7.9	0.80339	2.3	0.26	169.7641	8.9	1.54751	7.9	0.91
TSH-25-15.14	Thin section	2.0	0.7	2155.3	0.54	6.1	0.78651	1.3	0.38	199.4400	7.3	1.86366	6.1	0.83
TSH-25-15.15	Thin section	2.3	0.3	1721.4	0.80	6.1	0.79049	1.5	0.38	135.6749	7.3	1.24865	6.1	0.74
TSH-25-15.16	Thin section	3.6	1.0	3271.6	0.68	6.7	0.77514	2.2	0.39	155.2709	7.7	1.46729	6.7	0.80
TSH-25-15.18	Thin section	3.2	0.4	2280.5	0.86	6.8	0.79455	1.7	0.11	125.7219	7.9	1.16124	6.8	0.90
TSH-25-15.19	Thin section	2.9	1.2	2216.8	0.85	6.8	0.76590	2.2	0.42	122.5967	7.7	1.17741	6.8	0.78
TSH-25-15.20	Thin section	3.1	0.9	3019.8	0.67	6.0	0.79319	1.1	0.42	161.5584	7.2	1.48559	6.0	0.85
TSH-25-03.01	Thin section	7.8	0.3	1823.3	1.48	7.0	0.74516	2.3	0.28	68.4898	7.9	0.67467	7.0	0.82
TSH-25-03.02	Thin section	5.9	1.0	1500.5	1.38	6.7	0.74170	2.2	0.17	74.1676	8.0	0.72349	6.7	0.83
TSH-25-03.03	Thin section	5.5	0.2	980.8	1.91	6.7	0.72352	2.2	0.26	52.2070	7.8	0.52375	6.7	0.79
TSH-25-03.04	Thin section	33.2	0.2	2573.8	3.72	6.1	0.59259	1.3	-0.30	22.1261	7.5	0.26893	6.1	0.90
TSH-25-03.05	Thin section	23.1	0.1	2424.2	3.06	5.8	0.62996	1.1	0.29	28.2934	7.1	0.32632	5.8	0.71
TSH-25-03.06	Thin section	8.0	0.2	3584.9	0.95	6.3	0.79967	1.8	0.46	115.7563	7.4	1.05435	6.3	0.75
TSH-25-03.08	Thin section	15.1	0.1	4958.2	1.29	5.9	0.75833	0.8	0.39	80.8322	7.2	0.77313	5.9	0.85
TSH-25-03.09	Thin section	8.2	0.2	2181.8	1.61	6.0	0.72513	1.1	0.25	61.9325	7.2	0.62088	6.0	0.84
TSH-25-03.10	Thin section	108.7	0.6	20635.4	2.57	6.5	0.67043	1.3	0.27	35.8472	7.6	0.38852	6.5	0.91
TSH-25-03.11	Thin section	16.5	0.1	8069.1	1.36	6.4	0.75271	1.1	0.14	76.0329	7.4	0.73327	6.4	0.92
TSH-25-03.12	Thin section	13.2	0.1	7854.3	1.22	6.0	0.74935	1.2	0.46	84.5317	7.2	0.81927	6.0	0.81
TSH-25-03.13	Thin section	3.8	0.4	2514.6	1.24	6.0	0.75146	1.5	0.37	82.7656	7.2	0.80485	6.0	0.69
TSH-25-03.14	Thin section	4.8	0.1	4842.7	0.89	6.2	0.79302	1.7	0.40	122.5873	7.4	1.12642	6.2	0.76
TSH-25-03.15	Thin section	5.1	0.2	3749.8	1.23	5.9	0.75257	1.2	0.38	84.2327	7.2	0.81493	5.9	0.70
TSH-25-03.16	Thin section	7.7	0.2	6216.7	1.15	5.9	0.76152	1.0	0.37	90.8042	7.1	0.86769	5.9	0.74
TSH-25-03.17	Thin section	10.6	0.2	7212.8	1.35	5.9	0.74834	1.3	0.49	76.3704	7.1	0.74275	5.9	0.62
TSH-25-03.20	Thin section	9.0	0.2	4983.1	1.25	5.9	0.74751	1.2	0.42	82.3096	7.2	0.80202	5.9	0.68

f206 % =(207Pb/206Pbm - 207Pb/206Pb*)/(207Pb/206Pbc-207Pb/206Pb*)x100
if Age206Pb/238U < 1000Ma concordance % = (Age206Pb/238U / Age207Pb/235U) * 100 ; else concordance % = (Age207Pb/235U / Age207Pb/206Pb) * 100

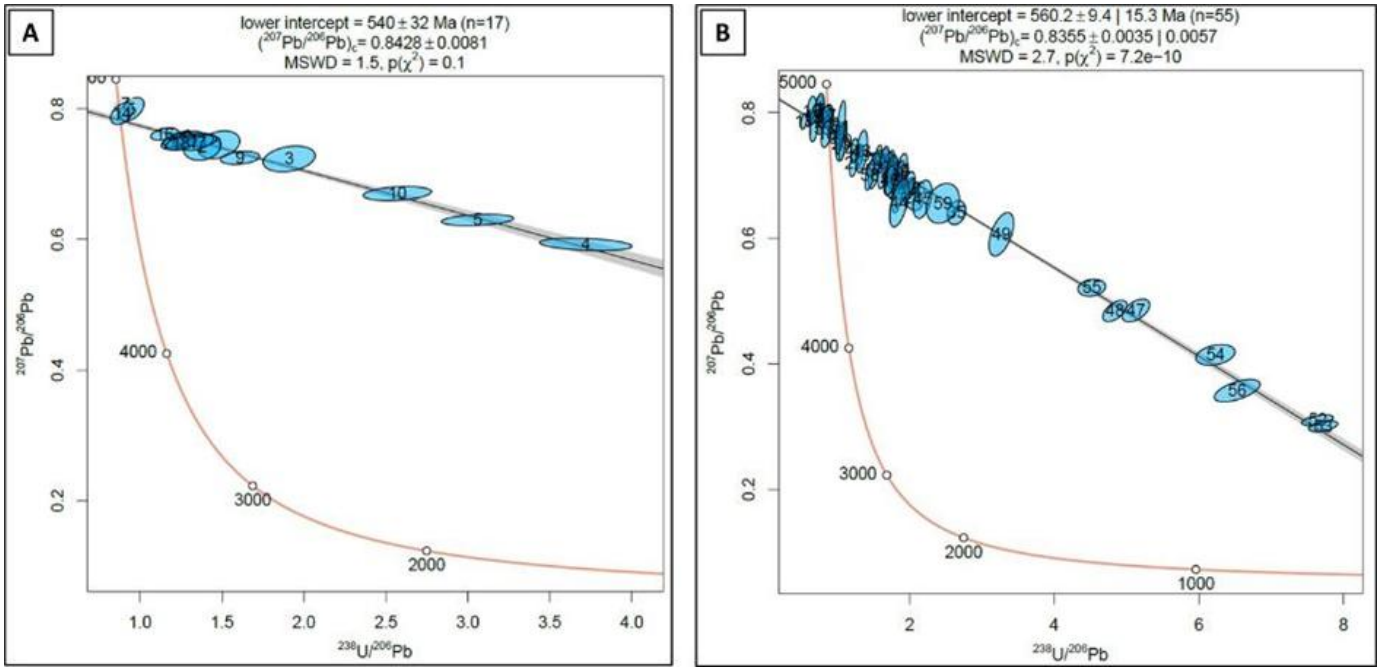


***Figure 11**: Tera–Wasserburg diagrams for U-Pb dating of titanite from the Lampa metarhyolites. **(A)** Tera-Wasserburg diagram of $^{207}Pb/^{206}Pb$ versus $^{238}U/^{206}Pb$ ratios for titanite analyses from sample TSH-25-03, yielding a lower-intercept age of 540 ± 32 Ma (n = 17). **(B)** Tera-Wasserburg diagram of $^{207}Pb/^{206}Pb$ versus $^{238}U/^{206}Pb$ ratios for titanite analyses from sample TSH-25-15, yielding a lower-intercept age of 560.2 ± 9.4 Ma (n = 55).*

5. Discussion

5.1. Petrographic heterogeneity and volcanic facies of the Lampa metarhyolites

The Lampa metarhyolites have been regarded as a succession of distinct effusive flows with internal petrographic variability **([16], [17]).**

The studied Lampa metarhyolites are not texturally homogeneous (Table 2). Petrographic observations (Figures 4-9) show that all samples preserve relict phenocrysts of "rhyolitic" quartz and feldspar, consistent with a rhyolitic protolith, however with variable tectono-metamorphic overprint. The phenocrysts enclosed within a fine-grained felsic groundmass define the primary volcanic fabric, whereas quartz recrystallization, feldspar sericitization, chloritization-epidotization and the development of foliation record subsequent metamorphism and deformation. The preservation of primary volcanic textures together with superimposed tectono-metamorphic fabrics is characteristic of many felsic metavolcanic successions and provides a reliable basis for reconstructing original volcanic facies despite later reworking **([2], [32], [33])**.

Based on the relative proportions of phenocrysts and felsic matrix, three volcanic facies are recognized (Figures 4-9): (i) matrix-rich metarhyolites, (ii) crystal-rich metarhyolites, and (iii) explosive facies (tuff). Matrix-rich metarhyolites are characterized by dispersed quartz and feldspar phenocrysts enclosed within a fine-grained felsic matrix, producing weakly porphyritic textures. In contrast, crystal-rich metarhyolites contain abundant quartz and feldspar phenocrysts, locally forming glomeroporphyritic crystal clusters, and display a markedly porphyritic texture. Variations in phenocryst abundance relative to the matrix are common in coherent felsic volcanic rocks and are generally interpreted as reflecting differences in magma crystallinity, crystal content and emplacement conditions rather than deformation alone **([2], [32], [33])**. Consequently, the textural differences observed among the metarhyolites most likely represent primary heterogeneity within the original rhyolitic volcanic succession in line with successive flows.

The distinctive tuff facies (sample TSH-25-43; Figure 9) differs from the coherent effusive metarhyolitic facies by preserving volcanic relict features that are absent from the other samples, including embayed quartz crystals, internal compositional layering and heterogeneity, locally preserved volcanic glass, internally fractured crystal fragments and possible glass shards (Figures 9D-E). Although these features have been modified by strong deformation, expressed by the well-developed foliation, locally affected by crenulation cleavage, together with the chlorite-rich matrix and porphyroclastic fabric (Figure 9C), their association is more consistent with a tuffaceous precursor than with tectonic processes alone. Similar relict textures have been reported from metamorphosed felsic tuff deposits in volcanic terranes, where primary pyroclastic features remain identifiable despite regional metamorphism and deformation **([2], [34], [33])**.

Although primary volcanic features are preserved, all facies have experienced variable tectono-metamorphic overprinting. Quartz recrystallization, feldspar sericitization, chloritization and epidotization, progressive alignment of phyllosilicates, foliation development and local porphyroclastic fabrics indicate that the original rhyolitic textures were modified to different degrees after emplacement. The intensity of this overprint varies considerably between samples, from weakly foliated metarhyolites that retain abundant primary volcanic textures

to strongly foliated rocks in which only relict volcanic fabrics remain.

Comparable relationships between preserved volcanic textures and superimposed tectono-metamorphic fabrics have been widely documented in deformed silicic volcanic successions **([7 – 9]).**

Overall, the petrographic evidence indicates that the Lampa metarhyolites comprise internally heterogeneous felsic volcanic facies that preserve significant elements of their original volcanic character despite subsequent Pan-African tectono-metamorphic overprinting. The recognition of matrix-rich, crystal-rich and pyroclastic facies refine previous descriptions of the unit. However, in the absence of detailed field mapping, the available petrographic data alone do not demonstrate whether these facies represent distinct eruptive units, successive volcanic flows or lateral facies variations within a single volcanic system.

Table 2. Summary of the petrographic characteristics of the volcanic facies identified within the Lampa metarhyolites. Diagnostic criteria are based on the relative abundance of quartz-feldspar phenocrysts and felsic groundmass, together with preserved volcanic textures and the nature of the tectono-metamorphic overprint.

Volcanic facies	Samples	Figures	Estimated proportions	Description criteria	Secondary tectono-metamorphic features	Interpretation
Matrix-rich effusive metarhyolites	TSH-25-03, TSH-25-54, TSH-25-56	Figs. 4-6	Groundmass: ~65-75%; quartz + feldspar phenocrysts: ~25–35%	Fine-grained felsic groundmass, dispersed quartz and feldspar phenocrysts, weakly porphyritic texture	Quartz recrystallization, feldspar sericitization, chlorite ± epidote, weak to moderate foliation	Coherent rhyolitic facies preserving a matrix-dominated volcanic texture
Crystal-rich effusive metarhyolites	TSH-25-15, TSH-25-63	Figs. 7-8	Groundmass: ~55-60%; quartz + feldspar phenocrysts: ~40-45%	Abundant quartz and feldspar phenocrysts, locally clustered crystals, distinctly porphyritic texture	Quartz recrystallization, sericitized feldspars, locally developed porphyroclastic texture	Coherent rhyolitic facies preserving a crystal-rich volcanic texture
Explosive pyroclastic facies (tuff)	TSH-25-43	Fig. 9	Fine pyroclastic matrix: ~65-70%; crystals and crystal fragments: ~30-35%	Embayed quartz, locally preserved volcanic glass, internally fractured crystal fragments and possible glass shards	Chlorite-rich foliated matrix, porphyroclastic fabric, crenulation cleavage and quartz microfractures	Metamorphosed felsic pyroclastic facies preserving relict volcanic textures

5.2. Titanite U-Pb geochronology and timing of the Pan-African tectono-metamorphic overprint

The titanite U-Pb data from the two Lampa metarhyolite samples define a coherent late Neoproterozoic age population. Samples TSH-25-03 and TSH-25-15 yield statistically indistinguishable Tera-Wasserburg lower-intercept ages of 540 ± 32 Ma and 560.2 ± 15.3 Ma, respectively, with a combined age of 559 ± 15 Ma (Figure 12). The consistency between the two samples suggests that these ages record a common geological event affecting the Lampa metarhyolites.

Petrographic and SEM observations indicate a secondary rather than primary magmatic origin for the dated titanite. In TSH-25-03, titanite occurs mainly as subhedral to anhedral grains dispersed within the recrystallized metarhyolitic matrix, whereas in TSH-25-15 it locally forms reaction rims and external overgrowths around ilmenite. These textures indicate titanite growth through reactions involving pre-existing Fe-Ti oxides during post-magmatic reworking. Uranium concentrations in the analyzed titanite are generally low (0.4-109 ppm), whereas Pb concentrations are comparatively high. Together with the coherent age populations obtained from both samples, the textural relationships support secondary titanite growth during post-magmatic reworking.

This interpretation is consistent with the secondary mineral assemblage observed in the Lampa metarhyolites, including chlorite, sericite and epidote, together with quartz recrystallization and feldspar sericitization. These mineralogical and textural features are consistent with the regional greenschist-facies tectono-metamorphic overprint previously recognized in the Lampa area (**[16], [17]**). No petrographic evidence for a higher-grade metamorphic overprint has been identified in the studied samples. We therefore interpret the 559 ± 15 Ma titanite age as recording

secondary titanite growth during regional greenschist-facies metamorphism and deformation associated with the Pan-African tectono-metamorphic evolution of the West Congo Belt, possibly assisted by fluid circulation.

The absence of zircon in our Lampa metarhyolite samples precludes direct determination of the crystallization age of the volcanic protolith. However, previous petrographic and geochemical data suggest a relationship with the felsic Inga/Lufu volcano-plutonic rocks of the Seke-Banza Group (**[16], [17]**). Moreover, within the WCB, the Lampa metarhyolites occur along strike between comparable felsic rocks of the Inga area (Kongo Central, DRC) and the Kakamoeka area (Republic of the Congo), for which Tonian magmatic ages of ca. 920-900 Ma have been reported (**[10], [11]**). The titanite ages therefore constrain a younger tectono-metamorphic event superimposed on this Tonian volcanic history rather than the timing of felsic magmatism itself.

At the regional scale, the 559 ± 15 Ma titanite age provides a new constraint on the timing of Pan-African tectono-metamorphic reworking in the Lampa area. In Kongo Central (DRC), it is compatible, within uncertainty, with the 566 ± 40 Ma $^{40}Ar/^{39}Ar$ age reported by Frimmel et al. (**[12]**) for regional metamorphism. Farther northwest, in the Republic of the Congo, Fullgraf et al. (**[35]**) distinguished two Pan-African tectono-metamorphic events, with a main M1 event at 590–570 Ma followed by a younger M2 event at 520–500 Ma. The M1 event represents the main phase of regional deformation and metamorphism during the Pan-African evolution of the West Congo Belt, whereas M2 records a later metamorphic overprint. Within analytical uncertainty, the 559 ± 15 Ma titanite age overlaps with the younger part of the M1 interval and is also consistent with the 566 ± 40 Ma regional age from Kongo Central. Regionally, the Pan-African metamorphic overprint ranges from greenschist-facies conditions to locally higher-grade, garnet-bearing assemblages (**[35]**,**[36]**). These regional constraints support interpretation of the Lampa titanite age as recording the local greenschist-facies expression of the main Pan-African tectono-metamorphic reworking of the West Congo Belt rather than an isolated thermal event. The new titanite U-Pb age thus provides a direct chronological constraint on Pan-African metamorphic reworking of the Lampa metarhyolites at ca. 560 Ma **(**Table 3)

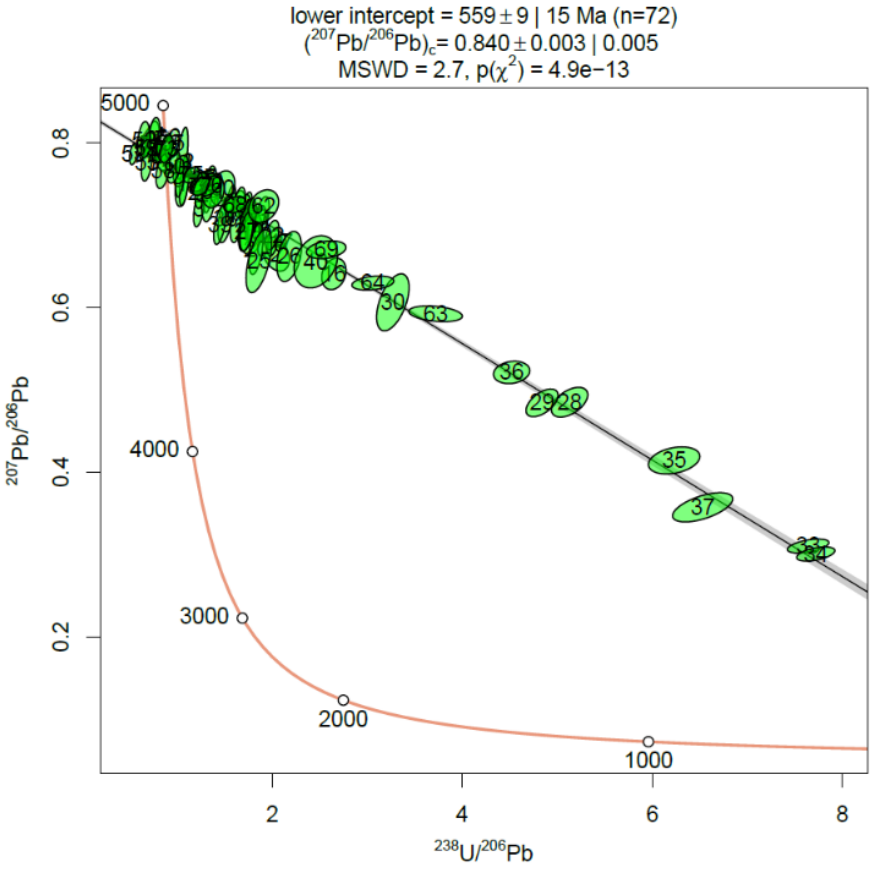


***Figure 12**: Combined Tera-Wasserburg U-Pb diagram ($^{207}Pb/^{206}Pb$ versus $^{238}U/^{206}Pb$) for titanite analyses from metarhyolite samples TSH-25-03 and TSH-25-15.*

Table 3: Selected geochronological constraints on the Pan-African tectono-metamorphic evolution of the West Congo Belt in the Democratic Republic of the Congo (DRC) and the Republic of the Congo (RoC).

Age (Ma)	Area	Rock unit	Dated mineral / Method	Geological significance	Reference
559 ± 15	Tshela area (DRC)	Lampa metarhyolites	Titanite U-Pb	Greenschist-facies Pan-African tectono-metamorphic reworking	**This study**
590–570	Mayombe region (RoC)	Regional metamorphic rocks	Illite–muscovite K-Ar	Main Pan-African regional metamorphism (M1)	Fullgraf et al. (2024)
566 ± 40	Kongo Central (DRC)	Tholeiitic feeder dolerite sill	Mafic minerals ($^{40}Ar/^{39}Ar$)	Regional greenschist-facies metamorphism and deformation	Frimmel et al. (2006)
520–500	Mayombe region (RoC)	Regional metamorphic rocks	Illite–muscovite K-Ar	Late Pan-African thermal event (M2)	Fullgraf et al. (2024)

6. Conclusion

This study presents an integrated petrological and *in situ* titanite U-Pb geochronological investigation of the Lampa metarhyolites (Inga Formation, Seke-Banza Group) from the Tshela area, southwestern Democratic Republic of the Congo. Based on fieldwork and petrological study, the unit appears to be internally heterogeneous, comprising matrix-rich metarhyolites, crystal-rich metarhyolites and distinctive explosive facies (rhyolitic tuff). The recognition of a pyroclastic facies, reported here for the first time within the Lampa metarhyolites, expands the spectrum of volcanic facies currently recognized in the Tshela felsic succession.

Titanite U-Pb analyses yield a combined lower-intercept age of 559 ± 15 Ma, providing the first direct geochronological constraint on Pan-African metamorphic reworking of the Lampa metarhyolites in the Tshela area. The consistency of this age across petrographically contrasting facies suggests that regional metamorphic recrystallization affected the volcanic succession while preserving significant elements of its original volcanic fabric.

Taken together, these findings support the interpretation that the Lampa metarhyolites represent an early Neoproterozoic (Tonian) felsic volcanic succession that was subsequently reworked during the WCB evolution. In the context of current knowledge on the Tshela area, this study refines the geological characterization of the unit by documenting its internal volcanic heterogeneity and providing its first direct metamorphic age constraint. These results establish a framework for future whole-rock geochemical, zircon U-Pb geochronological and regional stratigraphic studies, which will be essential for further constraining the origin, evolution and geodynamic significance of Tonian felsic magmatism preceding the formation of the West Congo Belt.

Acknowledgments

This research was conducted within the framework of the GeoRes4Dev (GeoResources for Development) project of the Royal Museum for Central Africa (RMCA, Tervuren, Belgium), funded by the Belgian Directorate-General for Development Cooperation (DGD). The authors gratefully acknowledge the support of the University of Kinshasa (UNIKIN) and the *Centre de Recherches Géologiques et Minières* (CRGM), particularly Prof. Holy HOLENU MANGENDA (UNIKIN) and Prof. Roland KAKULE KASEREKA (CRGM) for their assistance and logistical support.

The authors sadly acknowledge the passing of their co-author Prof. Albert TIENGE ONGENDANGENDA during the review process. The authors recognize his contribution to the project and his support during the early stages of this study.

References

[1] Boulter, C. A. (1993b), High-peperitic sills at Rio Tinto: Stratigraphic and mineralization implications, Trans. Inst. Min. Metall., 102,30 – 38.

[2] Mcphie, J., Doyle, M. and Allen, R. 1993: Volcanic Textures. A guide to the interpretation of textures in volcanic rocks. Tasmania, Tasmanian Government Printing Office, 196. pp.

[3] McPhie, J., DellaPasqua, F., Allen, S. R., & Lackie, M. A. (2008). Extreme effusive eruptions: Palaeoflow data on an extensive felsic lava in the Mesoproterozoic Gawler Range Volcanics. *Journal of Volcanology and Geothermal Research*, *172*(1–2), 148–161. https://doi.org/10.1016/j.jvolgeores.2006.11.011

[4] Skilling, I. P. (2002). Basaltic pahoehoe lava-fed deltas: Large-scale characteristics, clast generation, emplacement processes and environmental discrimination. *Geological Society, London, Special Publications*,*202*(1),91–113. https://doi.org/10.1144/GSL.SP.2002.202.01.06

[5] Gaboury, D., & Pearson, V. (2008). Rhyolite Geochemical Signatures and Association with Volcanogenic Massive Sulfide Deposits: Examples from the Abitibi Belt, Canada. *Economic Geology*, *103*(7),1531–1562. https://doi.org/10.2113/gsecongeo.103.7.1531

[6] Khalaf, E. A., Abdel Motelib, A., Hammed, M. S., & El Manawi, A. H. (2015). WITHDRAWN: Volcano-sedimentary characteristics in the Abu Treifiya Basin, Cairo–Suez District, Egypt: Example of dynamics and fluidization over

sedimentary and volcaniclastic beds by emplacement of syn-volcanic basaltic rocks. *Journal of Volcanology and Geothermal Research*, *292*,1–28. https://doi.org/10.1016/j.jvolgeores.2015.01.001

[7] Vernon, R. H. (2004). *A Practical Guide to Rock Microstructure* (1st ed.). Cambridge University Press. https://doi.org/10.1017/CBO9780511807206

[8] Passchier, C.W. and Trouw, R.A. (2005) Microtectonics. Springer-Verlag, Berlin, 366 p.

[9] Bucher, K., & Grapes, R. (2011). *Petrogenesis of Metamorphic Rocks*. Springer Berlin Heidelberg. https://doi.org/10.1007/978-3-540-74169-5

[10] Tack, L. (2001). Early Neoproterozoic magmatism (1000–910 Ma) of the Zadinian and Mayumbian Groups (Bas-Congo): Onset of Rodinia rifting at the western edge of the Congo craton. *Precambrian Research*, *110*(1–4), 277–306. https://doi.org/10.1016/S0301-9268(01)00192-9

[11] Tack, L., Fernandez-Alonso, M., Baudet, D., De Grave, J., Nseka-Mbemba, P., & Pedrosa-Soares, A. C. (2024). Anorogenic plutonism in the West Congo Belt of the Democratic Republic of Congo further supports early Tonian continental rifting in the Congo – São Francisco palaeocontinent. *Journal of African Earth Sciences*,*215*,105273. https://doi.org/10.1016/j.jafrearsci.2024.105273

[12] Frimmel, H. E., Tack, L., Basei, M. S., Nutman, A. P., & Boven, A. (2006). Provenance and chemostratigraphy of the Neoproterozoic West Congolian Group in the Democratic Republic of Congo. *Journal of African Earth Sciences*, *46*(3), 221–239. https://doi.org/10.1016/j.jafrearsci.2006.04.010

[13] De Grave, J., Glorie, S., Archibald, D. B., Tack, L., Baudet, D., Theunissen, K., Nseka-Mbemba, P., & Love-Pay, A. (2026). Incipient formation of the African precursor basin to the Ediacaran-Cambrian Araçuaí − West Congo Orogen: Implications for Columbia breakup and Gondwana assembly. *Gondwana Research*, *149*, 445–464. https://doi.org/10.1016/j.gr.2025.08.013

[14] Alvarez P (1995a) Les facteurs de contrôle de la sédimentation du Supergroupe Ouest-congolien (Sud-Congo). Rampe carbonatée et activité biologique au Protérozoïque supérieur. Implication en Afrique centrale (Congo, Zaïre, Gabon, Cameroun, Guinée Equatoriale, Centrafrique). Document BRGM, 239, 273 p.

[15] Alvarez P (1995b) Evidence for a Neoproterozoic carbonate ramp on the northern edge of the Central African Craton: relations with Late Proterozoic intracratonic troughs. Geol Rund 84:636-648

[16] Tack, L., 1975. Bijdrage tot de studie van de geologie, de petrografie en de petrologie van het Mayumbiaan van Neder-Zaïre. Unpublished Ph.D. Thesis, Ghent University (Belgium), 200 pp. + annexes.

[17] Tack, L. (1979), Etude pétrochimique du Mayumbien au Bas-Zaïre : une séquence volcano-plutonique acide précambrienne, Annales du Musée Royal de l'Afrique Centrale, Tervuren, Belgique, Série in-8°, Sciences Géologiques, vol. 84, xiv + 56 pp.

[18] De Waele, B., Johnson, S. P., & Pisarevsky, S. A. (2008). Palaeoproterozoic to Neoproterozoic growth and evolution of the eastern Congo Craton: Its role in the Rodinia puzzle. *Precambrian Research*, *160*(1–2), 127–141. https://doi.org/10.1016/j.precamres.2007.04.020

[19] Delhal, J. et Ledent, D. (1976). Age et évolution comparée des geniss migmatitiques Pré-Zadinniens des régions de Boma et de Mpozo-Tombagadio. Ann. Soc. Géol. Bel., 99, 165-187.

[20] Cahen, L., Snelling, N. J., Delhal, J. and Vail, J. R. (1984). The Geochronology of Africa. Clarendon Press, Oxford, 512pp.

[21] Love Pay, A. L. P., François, C., Delvaux, D., Nkodia, H., Poujol, M., Vandenbroecke, G., Baudet, D., Kanda, V., Kitambala, N., & Tack, L. (2026). Pétrologie et géochronologie des marbres paléoprotérozoïques du supergroupe de kimeza dans la région de matadi (Province du Kongo Central, R.D. Congo). *Journal Africain Des Sciences*, *3*(5), 1–18. https://doi.org/10.70237/jafrisci.2026.v3.i5.

[22] Johnson, S. P., Rivers, T., & De Waele, B. (2005). A review of the Mesoproterozoic to early Palaeozoic magmatic and tectonothermal history of south–central Africa: Implications for Rodinia and Gondwana. *Journal of the Geological Society*, *162*(3), 433–450. https://doi.org/10.1144/0016-764904-028

[23] Tack, L. (1973). Le massif de la Lufu et sa bordure (République du Zaïre). Note préliminaire. *Annales de la Société géologique de Belgique*, 96, 1, 31–47.

[24] Delpomdor, F., Kant, F., Tack, L., & Préat, A. (2019). Cyclicity and sequence stratigraphy of the Neoproterozoic uppermost Haut Shiloango-Lukala carbonate ramp system in the Lower Congo region (Democratic Republic of the Congo): Example of tectonostratigraphic control versus climatic changes. *Journal of African Earth Sciences*, *160*, 103636. https://doi.org/10.1016/j.jafrearsci.2019.103636

[25] Tait, J., Straathof, G., Söderlund, U., Tack, L., Ernst, R., Kanda Nkula, V. and Cibambula, E., 2010. The Sumbi-type sills of Western Congo ("Bas-Congo" region, Democratic Republic of Congo, DRC): New constraints for the Neoproterozoic rifting and the Lower Diamictite Unit of the West Congo Belt. Confidential report A16. Www.supercontinent.org.

[26] Straathof, G.B., 2011. Neoproterozoic Low Latitude Glaciations: An African Perspective. Ph.D. Thesis, University of Edinburgh. Uitgeverij BOXPress, Oisterwijk, The Netherlands, 283 pp.

[27] Archibald, D., Glorie, S., Muanza-Kant, P., Baudet, D., Kanda-Nkula, V., Kitambala-Yaya, N., Mpiana-Kenababo, C., Nseka-Mbemba, P., Tack, L., 2018. The lower Diamictite Formation of the Cataractes Group, West Congo Supergroup (Bas-Congo region, DR Congo): a 678 Ma marker of extensional episodic activity during breakup of Columbia. In: 17th Conference of the Geological Society of Africa and 27th Colloquium of African

Geology, Aveiro, Portugal. Book of Abstracts, p. 19.

[28] Van Ranst, G., Fonseca, A. C., Tack, L., Delvaux, D., Baudet, D., Kitambala, N. Y., Pay, A. L., & De Grave, J. (2022). Exhumation of the passive margin of the DR Congo during pre- and post-Gondwana breakup: Evidence from low-temperature thermochronology, geology and geomorphology. *Geomorphology*,*398*,108067. https://doi.org/10.1016/j.geomorph.2021.108067

[29] Paton, C., Woodhead, J. D., Hellstrom, J. C., Hergt, J. M., Greig, A., & Maas, R. (2010). Improved laser ablation U-Pb zircon geochronology through robust downhole fractionation correction. *Geochemistry, Geophysics, Geosystems*, *11*(3), 2009GC002618. https://doi.org/10.1029/2009GC002618

[30] Kennedy, A. K., Kamo, S. L., Nasdala, L., & Timms, N. E. (2010). Grenville skarn titanite: potential reference material for sims u-th-pb analysis. *The Canadian Mineralogist*, *48*(6), 1423–1443. https://doi.org/10.3749/canmin.48.5.1423

[31] Schoene B., Crowley J.L., Condon D.J., Schmitz M.D. and Bowring S.A. (2006). Reassessing the uranium decay constants for geochronology using ID-TIMS U-Pb data. Geochimica et Cosmochimica Acta, 70, 426–445p.

[32] Doyle, M. G. (2001). Volcanic Influences on Hydrothermal and Diagenetic Alteration: Evidence from Highway-Reward, Mount Windsor Subprovince, Australia. *Economic Geology*, *96*(5), 1133–1148. https://doi.org/10.2113/gsecongeo.96.5.1133

[33] Gifkins, C. C., Allen, R. L., & McPhie, J. (2005). Apparent welding textures in altered pumice-rich rocks. *Journal of Volcanology and Geothermal Research*,*142*(1–2),29–47. https://doi.org/10.1016/j.jvolgeores.2004.10.012

[34] Branney MJ, Kokelaar P (2002) Pyroclastic density currents and sedimentation of ignimbrites. Geol Soc London (Mem) 27 :1–138

[35] Fullgraf, T., Callec, Y., Bauer, H., Boudzoumou, F., Charles, N., Gloaguen, E., Issautier, B., Kebi, S. T., Le Bayon, B., Le Metour, J., Paquet, F., Sergeev, S., & Wemmer, K. (2024). Structural architecture and metamorphism of the Mayombe Chain and Niari Basin (West Congo Belt) in Congo Brazzaville. *Journal of African Earth Sciences*, *220*, 105369. https://doi.org/10.1016/j.jafrearsci.2024.105369

[36] Bouenitela, V.T.T., 2019. Le domaine Paléoprotérozoïque (éburnéen) de la chaîne du Mayombe (Congo-Brazzaville) : origine et évolution tectono-métamorphique. Thèse 3eme Cycle. Universit´e Rennes, France, p. 448.